Sol-gel synthesis and the effect of boron addition on the phosphorescent properties of $SrAl_2O_4:Eu^{2+},Dy^{3+}$ phosphors

I-Cherng Chen and Teng-Ming Chen[a)]
Institute of Applied Chemistry, National Chiao Tung University, Hsinchu 30050, Taiwan, Republic of China

(Received 10 October 2000; accepted 22 November 2000)

The effects of boron addition on the microstructure and afterglow properties of the long-phosphorescent $SrAl_2O_4:Eu^{2+},Dy^{3+}$ (SAED), synthesized via a novel sol-gel route, were systematically investigated. Significant improvement on luminescence intensity and the lengthening of afterglow persistent time in boron-added SAED (BSAED) phases were observed, as compared to those without boron addition and commercial phosphors. Typical bluish-green emissions attributed to the doublet phosphorescence with wavelengths peaking at 412 and 501 nm for BSAED phase and 398 and 486 nm for the pristine SAED phase were observed. Afterglow with wavelengths peaking at 403 and 485 nm was observed for BSAED phase, whereas that with wavelengths peaking at 486.5 nm was found for the pristine SAED phase, as indicated by time-dependent afterglow decay profiles. Results from scanning electron microscopic morphological studies were used to investigate the modification of microstructure of the BSAED phases.

I. INTRODUCTION

Eu^{2+}-activated alkaline earth aluminates are known as phosphorescent phosphors for their high quantum efficiency in the visible region as indicated in investigations on the $MAl_2O_4:Eu^{2+}$ and $MAl_{12}O_{19}:Eu^{2+}$ (M = Ca, Sr, Ba) phases described by Blasse *et al.*[1] Palilla *et al.* investigated the phosphorescent properties of $SrAl_2O_4:Eu^{2+}$ green phosphor with emission wavelength (λ_{em}) of 520 nm and attributed the phosphorescence to the $4f^6 5d \rightarrow 4f^7$ transition of Eu^{2+}.[2] Later, the Eu^{2+}- and Dy^{3+}-coactivated $SrAl_2O_4$ (SAED) phase with tridymite-type structure was reported by Murayama *et al.*[3] to exhibit long persistent and bright bluish-green phosphorescence and greater chemical stability than traditional sulfide-based ZnS:Cu,Co phosphors. Thus $SrAl_2O_4:Eu^{2+},Dy^{3+}$ has been considered as a useful bluish-green phosphor for use in dials for luminous watches and clocks as well as a potential outdoor nighttime display. However, basing their conclusions on the investigations of the phosphorescence, thermoluminescence, and photoconductivity characteristics of polycrystalline $SrAl_2O_4:Eu^{2+},Dy^{3+}$, Matsuzawa *et al*. suggested a mechanism indicating that the phosphorescence is caused by the presence of holes and to the trapping and thermal release of holes by Dy^{3+} ions in the system.[4]

Furthermore, Katsumata *et al.*[5] studied the host composition effect on the phosphorescent properties of SAED crystals by varying the mole ratio of Al/Sr (from 2.05 to 2.22) and Dy/Eu (from 0 to 3.55). They concluded that λ_{em} attributed to Eu^{2+} ions did not vary with the host and/or activator compositions.[5] On the contrary, Sakai *et al.* investigated the effect of composition on the phosphorescence of $BaAl_2O_4:Eu^{2+},Dy^{3+}$ crystals and concluded that the intensity of afterglow phosphorescence, the trap depth, and the trap density derived from the thermoluminescence measurements vary with the host compositions.[6] Jia *et al.* reported the measurements of phosphorescence and decay dynamics for both $SrAl_2O_4:Eu^{2+}$ and $SrAl_2O_4:Eu^{2+},Dy^{3+}$ single crystals.[7] Their results indicated that the trapping rate of Dy^{3+} ions is fast with efficiency of about 40% at ambient temperature, and the decay curves of afterglow are nonexponential and cannot be explained simply by thermally activated detrapping processes.

Apparently, long-lasting phosphorescent $MAl_2O_4:Eu^{2+},Dy^{3+}$ (M = Ca, Sr, Ba) phases have been of great interest to a number of investigators and have been actively investigated from the perspectives of both materialistic and mechanistic views, as indicated by the works described above. However, without flux the preparation of SAED phases generally requires high temperature (i.e., 1400 to 1600 °C) by solid-state reactions,[8,9] but the addition of B_2O_3 was proven by Pet *et al.* to effectively lower the processing temperature (i.e., 1100 to 1500 °C) in the preparation of another analogue $Sr_4Al_{14}O_{25}:Eu^{2+}$.[10]

a)Address all correspondence to this author.
e-mail: tmchen@cc.nctu.edu.tw

Therefore, the present work was motivated by the possibility of developing a new route for synthesizing phosphorescent SAED phosphors with, hopefully, higher brightness and longer afterglow persistent time and by the possibility of acquiring optimal materials parameters for the applications of long-lasting phosphors. In this paper we report a sol-gel synthetic route with lower processing temperature by employing an alkyl borate as a source of flux as well as metal-alkoxide precursors for the formation of $SrAl_2O_4:Eu^{2+},Dy^{3+}$. We investigated the photoluminescence (PL), afterglow profiles, and afterglow decay rates. We also compared the microstructure of as-prepared polycrystalline SAED phases with or without boron addition. Attempts to rationalize our observations were based on the variation in coordination environment of Eu^{2+} and microstructure modifications attributed to boron addition.

II. EXPERIMENTAL

The sol-gel process utilized to synthesize $SrAl_2O_4$:Eu,Dy phosphors is summarized in the flow diagram represented in Fig. 1. Briefly, we prepared solution I by dissolving 4.2 g of aluminum isopropoxide (98%, Strem Chemicals, Newburyport, MA), and refluxing at 110 °C for 1 h in 100 ml of 2-methoxyethanol (99%, Merck, Darmstedt, Germany), to which 0.45 g of trimethylborate (98%, Strem Chemicals) was then added. We prepared solution II by dissolving nitrates of Sr, Eu, and Dy (all 99.9%, Aldrich Chemicals, Milwaukee, WI), with a stoichiometry of 1:0.05:0.05 in a mixture of 2-methoxyethanol and deionized water in a 50:50 vol% proportion. To avoid the hydrolysis of cations and boron alkoxides before mixing, we added 3 g of ethylacetoacetate (EAA) into solution I as a chelating agent before mixing solutions I and II. Solutions I and II were then mixed well by constant stirring and kept in an ice bath to activate the gel formation.

Several trial stoichiometries of $Sr:Al:Eu:Dy:B(OEt)_3$ were attempted in the synthesis, and the optimal stoichiometry was determined and will be reported elsewhere.[11] However, the molar stoichiometry adopted in this work was 1:2:0.05:0.05:0.3 for $Sr:Al:Eu:Dy:B(OEt)_3$.

The resulting white gels were then dried at 80 to 120 °C for 5 h, heated at temperatures between 500 and 1200 °C for 10–24 h, and finally reduced at 1300 °C under an atmosphere of H_2/N_2 (5%:95%) for 1 h to assure complete conversion of Eu^{3+} to Eu^{2+}.

The synthetic conditions for all the boron-free and boron-added $SrAl_2O_4$:Eu,Dy (SAED and BSAED) samples investigated in this work are summarized in Table I.

A small portion (20 mg) of resulting gels of SAED and BSAED was dried at 150 °C and characterized by differential thermal analysis (DTA) at the heating rate of 5 °C/min using a Du Pont 1600 thermal analysis system (DuPont Instruments, Wilmington, DE).

The phase purity and homogeneity of the as-prepared SAED and BSAED samples were investigated by x-ray diffraction (XRD). The XRD profile data for the $SrAl_2O_4:Eu^{2+},Dy^{3+}$ phases were collected with a MAC Science MXP-3 automatic diffractometer (MAC Science Co., Ishigawa, Japan) with a graphite-monochromatized and Ni-filtered Cu K_α radiation. Special caution was taken to make sure that no starting material or any other impurity phase was identified in the XRD profiles.

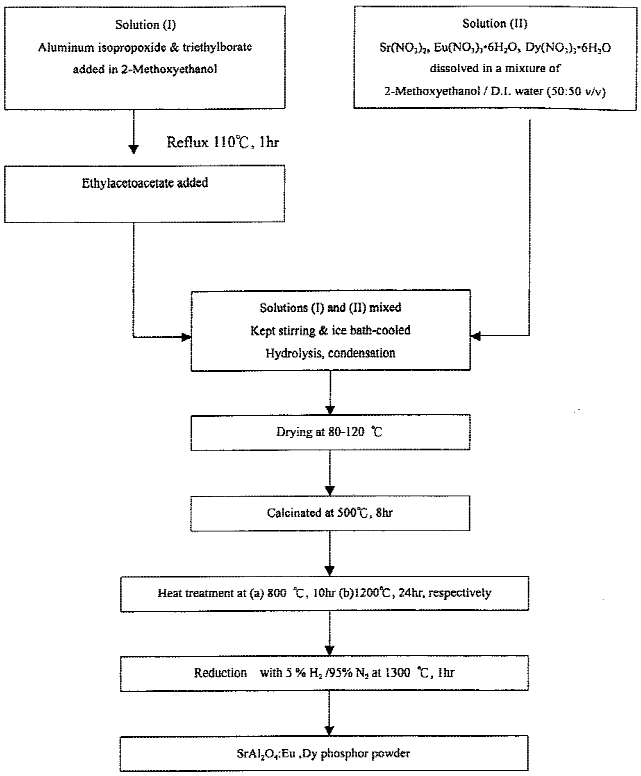

FIG. 1. Flow diagram for the synthesis of $SrAl_2O_4$:Eu,Dy via a sol-gel route.

TABLE I. The preparation conditions or sources for $SrAl_2O_4$:Eu,Dy samples investigated in this work.

Samples	Conditions of preparation or sources
SAED-LT	Boron-free, preheated at 800 °C for 10 h and reduced at 1300 °C under 5% H_2 for 1 h.
SAED-HT	Boron-free, preheated at 1200 °C for 24 h and reduced at 1300 °C under 5% H_2 for 1 h.
BSAED-LT	Boron-added, preheated at 800 °C for 10 h and reduced at 1300 °C under 5% H_2 for 1 h.
BSAED-HT	Boron-added, preheated at 1200 °C for 24 h and reduced at 1300 °C under 5% H_2 for 1 h.
LumiNova® BG-300M	Commercialized $Sr_4Al_{14}O_{25}$:Eu, Dy phosphor patented by Nemoto Co., Japan[3]

The morphological investigations of the as-prepared polycrystalline $SrAl_2O_4:Eu^{2+},Dy^{3+}$ were carried out with a CamScan 4D scanning electron microscope (SEM; CamScan Electron Optics Co., Cambs, UK). Measurements of PL spectra were carried out under ultraviolet excitation ($\lambda_{exc} = 270$ nm) with a Shimadza RF-5301PC spectrophotometer equipped with a 150-W xenon lamp as an excitation source and an R928-type photomultiplier as a detector. The polycrystalline phosphor powders were compacted into a cylindrical dish groove (10 mm diameter × 5 mm length) of a holder that was then transferred to the spectrophotometer.

On the other hand, prior to the measurements of afterglow curves and afterglow decay profiles, the $SrAl_2O_4:Eu^{2+},Dy^{3+}$ samples were stored in a dark chamber for 8 h to avoid the interference from pre-activating light. The samples were then irradiated with ultraviolet light ($\lambda = 270$ nm) for 30 min. The initial intensity of phosphorescence defined as *I*INFo was measured approximately 1 s after the excitation was terminated. Moreover, the time-dependent phosphorescence intensity (I) was measured at emission wavelength of 485 ± 2 nm in a dark chamber with excitation source turned off.

III. RESULTS AND DISCUSSION

A. Sol-gel synthesis and DTA studies on precursors

As indicated in Fig. 1, the pristine (SAED) and boron-added $SrAl_2O_4:Eu^{2+},Dy^{3+}$ (BSAED) phases can be synthesized via a sol-gel route at about 1200 °C, which is relatively lower than that (i.e., 1400 to 1600 °C) adopted by solid-state reactions without adding fluxes[8,9] or that (1100 to 1500 °C) adopted by synthetic routes with addition of B_2O_3.[10] The addition of ethylacetoacetate into solution I prior to the mixing of solutions I and II was attempted to inhibit the undesirable precipitation of gelatinous $Al(OH)_3$ due to hydrolysis of aluminum isopropoxide by forming metal chelates.[12]

To track the formation temperature for strontium aluminates during heat treatment and determine effective conditions for preparation, the precursors for SAED and BSAED phases were characterized by DTA in the range of 400 and 1200 °C, and the results are shown in Figs. 2(a) and 2(b), respectively. The endothermic peak at 596 ± 2 °C can presumably be attributed to the formation of $SrCO_3$ and hydrous $Al(OH)_3$, as indicated by the analysis of XRD profiles. The relatively broad endothermic band observed at temperature between 890 and 1200 °C for BSAED was attributed to the formation of strontium borates and/or $SrAl_2O_4$ phases, as compared to the DTA profile for SAED represented in Fig. 2(a).

B. XRD phase analysis

The XRD profiles for as-prepared $SrAl_2O_4$:Eu, Dy samples derived from various synthetic conditions, namely, SAED-low temperature (LT), SAED-high temperature (HT), BSAED-LT, BSAED-HT, and LumiNova®BG-300M (a commercialized $Sr_4Al_{14}O_{25}$:Eu,Dy phosphor patented by Nemoto Co., Tokyo, Japan[3]) are shown in Figs. 3(a)–3(e).

The XRD profile for SAED-LT exhibiting weak blue greenish phosphorescence was found to contain mainly $Sr_3Al_2O_6$ and $SrAl_2O_4$ in minor proportion. In contrast, that for SAED-HT, synthesized at higher sintering temperature than SAED-LT, was found to contain mostly $SrAl_2O_4$ and a small amount of $SrAl_{12}O_{19}$, as indicated by the analysis of Figs. 3(a) and 3(b). Furthermore, we found that the BSAED phase, synthesized from a starting composition of 1:2:0.05:0.05:0.1 for Sr:Al:Eu:Dy:$B(OEt)_3$ and reduced under an atmosphere of H_2/N_2 at 1300 for 1 h, exhibits typically blue-green

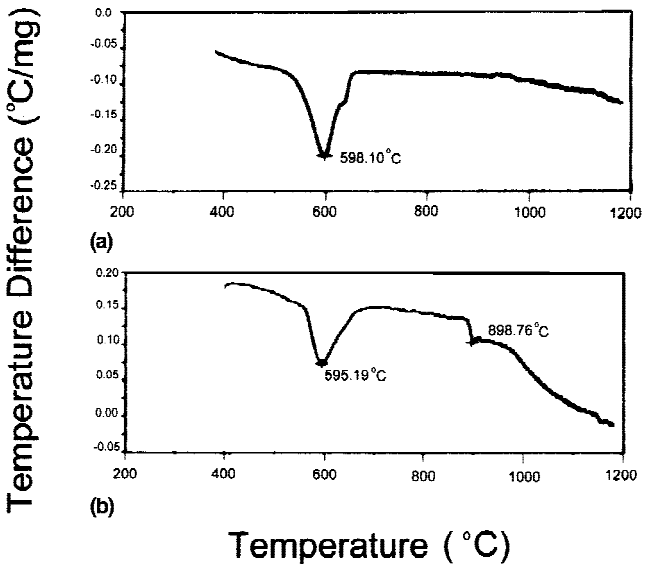

FIG. 2. DTA profiles for precursors of (a) SAED and (b) BSAED synthesized via a sol-gel route

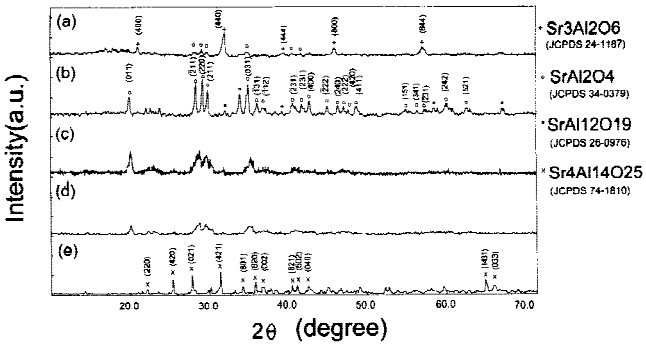

FIG. 3. XRD profiles for (a) SAED-LT, (b) SAED-HT, (c) BSAED-LT, (d) BSAED-HT, and (e) BG-300M.

afterglow. The BSAED phase was also observed to be poorly crystalline and probably coexists with a small amount of glassy strontium borates formed from Sr^{2+} and $B(OEt)_3$ (precursor of B_2O_3 that also acts as a flux), as indicated by the XRD profile shown in Fig. 3(d).

In fact, we observed that the $Sr_3Al_2O_6$ phase dominates in the products obtained from reactions with a starting Al/Sr molar ratio below 2, whereas $SrAl_{12}O_{19}$ exists as a major phase in those with Al/Sr ratio ranging from 5 to 12 .[11] However, the reduction of activator Eu^{3+} into Eu^{2+} under H_2/N_2 atmosphere (5:95 vol%) at 1300 °C was always found to be essential for the as-prepared SAED phases to exhibit phosphorescence and afterglow of decent intensity. The XRD profile for the commercial phosphor BG-300M was also investigated and represented in Fig. 3(e) for comparison. We found that BG-300M mainly contained $Sr_4Al_{14}O_{25}$:Eu,Dy (JCPDS card no. 74-1810), but not monoclinic $SrAl_2O_4$:Eu,Dy, as indicated by the XRD profile shown in Fig. 3(e).

C. Microstructure investigations

The SEM micrographs for as-prepared SAED-HT and BSAED-LT, BG-300M, and BSAED-HT are shown in Figs. 4(a)–4(d), respectively. Irregularly spherical grains with sizes of several tenths of a micron to several microns were observed in as-prepared boron-free SAED-HT, whereas the boron-added BSAED-LT shown in Fig. 4(b) exhibited irregularly rectangular grains with partially melting morphology. The grain boundaries observed in BSAED-LT with partially melting character can be barely unambiguously recognized. The observed differences between the microstructures of SAED-HT and BSAED-LT phases can presumably be attributed to the pretreatment temperature and reaction durations (i.e., at 1200 °C for 24 h adopted in the former versus 800 °C for 10 h in the latter) and, most importantly, to the effect of boron addition. We found that the addition of boron provides a low melting medium of metal borates for the reaction to proceed and, consequently, accelerates the formation of $SrAl_2O_4$:Eu,Dy phases, as indicated by Fig. 4(b).

On the other hand, the SEM micrograph for the commercially available BG-300M represented in Fig. 4(c) exhibits irregular grain morphology and slightly partial melting character, extremely similar to that observed in BSAED-LT whose SEM micrograph is also shown in Fig. 4(b). However, the microstructure of boron-added BSAED-HT (presintered at 1200 °C for 24 h and then reduced at 1300 °C for 1 h) shown in Fig. 4(d) was found to exhibit a completely melting character that was commonly observed for phosphor synthesis employing boric acid or borates as a flux.

The partial melting character observed in the microstructure of BSAED-LT and BSAED-HT could presumably be attributed to the formation of a layer of low-density borates floating on the surface of bulk reactants.

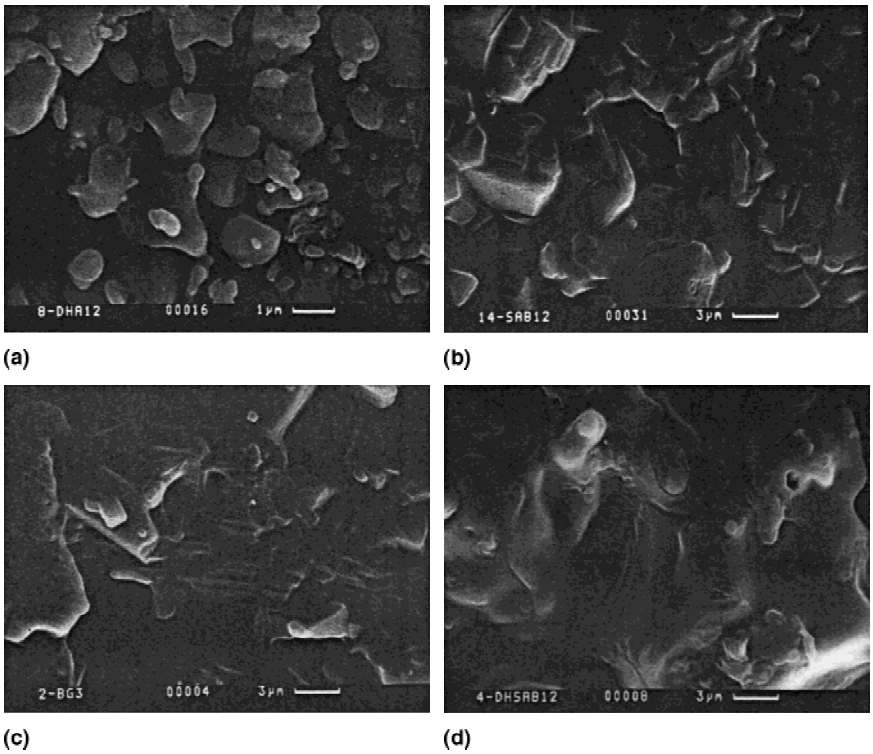

FIG. 4. Comparison of SEM microstructure for (a) SAED-HT, (b) BSAED-LT, (c) BG-300M, and (d) BSAED-HT.

D. Reduction of Eu^{3+} on boron addition

The reduction of Eu^{3+} to Eu^{2+} was observed in the synthesis of BSAED, even when synthesized at 1300 °C in air. This observation of partial reduction on Eu^{3+} is consistent with the afterglow curve and PL spectra represented in Fig. 5 for BSAED phases. The twin peaks at 405 and 485 nm observed in the afterglow curve shown in Fig. 5(a) are attributed to Eu^{2+} ($4f^6 5d \rightarrow 4f^7$) of BSAED-LT, whereas the emission peaks at 589, 612, and 680 nm are attributed to the Eu^{3+} $^5D_0 \rightarrow {}^7F_{J=1\ to\ 3}$ multiplets[13] and Eu^{2+} $4f^6 5d \rightarrow 4f^7$ transition, as indicated by PL spectra shown in Fig. 5(b). The host of boron-modified $SrAl_2O_4$ (BSAED) consists of a nonhomogeneous composite that includes mostly $SrAl_2O_4$ and a minor proportion of glassy strontium borates formed from SrO and B_2O_3. Pei *et al.*[14] proposed a substitution defect model that states nonequivalent substitution of Eu^{3+} for Sr^{2+} creates electrons on Sr^{2+} vacancies in strontium borates. The anionic BO_4^{5-} tetrahedra of metal borates were believed to play an important role of electron transfer in the reduction process of Eu^{3+} to Eu^{2+}, and the network of BO_4^{5-} tetrahedra may also act as a shield to prevent oxygen diffusion. Machida *et al.*[15] suggested that the concentration quenching effect in Eu^{2+}-activated Sr-borates could be expected to be lowered by a shielding effect of the BO_4^{5-} network for Eu^{2+}–Eu^{2+} interaction. Consequently, boron addition in the synthesis of SAED in fact favors the formation of Eu^{2+} whose presence has been proven to be essential for BSAED or SAED phases to exhibit long phosphorescence characteristics.[4,5]

E. Photoluminescence spectra

The PL emission spectra excited at λ_{exc} of 270 nm for samples SAED-HT, BSAED-LT, and BG-300M are shown in Figs. 6(a) to 6(c), respectively. Broad doublet

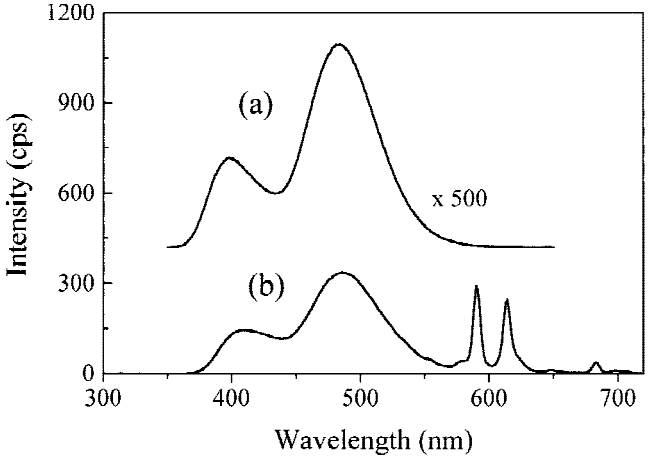

FIG. 5. Effect of Eu^{3+} reduction in a borate matrix on (a) afterglow curve and (b) PL emission spectra for boron-added BSAED sample (λ_{exc} = 270 nm).

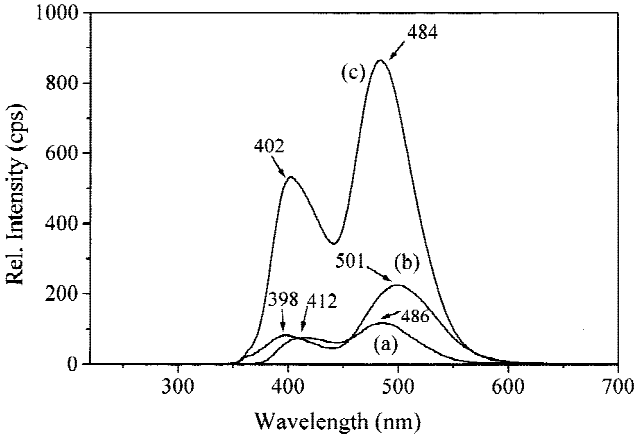

FIG. 6. Photoluminescence spectra (λ_{exc} = 270 nm) for (a) SAED-HT, (b) BSAED-LT, and (c) BG-300M.

emission bands peaking at different λ_{em}'s attributed to the typical $4f^6 5d^1 \rightarrow 4f^7$ transitions of Eu^{2+} were observed for all three samples. However, the observed λ_{em}'s for the three samples were found to be shorter than that (i.e., λ_{em}at 520 nm) of the SAED phase reported by Matsuzawa *et al.*[4] The observed discrepancy in shifting of λ_{em}'s may probably be attributed to the difference in the crystal field strength that Eu^{2+} experienced and inherited from different preparation routes. The SAED and boron-modified BSAED samples derived from a sol-gel process were found to be less crystalline than those synthesized from solid state reactions. Moreover, the $4f^6 5d$ state of Eu^{2+} has been observed to be sensitive to the strength of crystal field,[16,17] and it may split into sublevels depending on the strength of the crystal field. On the other hand, with decreasing crystal field strength, the luminescence for Eu^{2+} from different sublevels was found to exhibit red to blue.[18] In $SrAl_2O_4$ with β-tridymite structure (monoclinic $P2_1$ space group) Sr^{2+} ions are located in the cavities of the framework of AlO_4^{5-} tetrahedra. Using the structural study of polycrystalline $SrAl_2O_4$ by Schulze *et al.*,[19] we were able to identify Sr^{2+} in two different sites with low symmetry and coordinated by nine oxygen atoms. Eu^{2+} ions are likely to substitute for the Sr^{2+} sites because of the similarity in ionic radius, and this explains the observed twin peaks in Eu^{2+}-activated $SrAl_2O_4$ or $Sr_4Al_{14}O_{25}$ phase. In particular, Eu^{2+} is considered to be located in a poorly crystalline as well as nonhomogeneous host environment with at least two types of coordination, as suggested by XRD, SEM, and PL data for SAED-HT and BSAED-LT. Furthermore, the commercially available LumiNova®BG-300M (i.e., $Sr_4Al_{14}O_{25}$:Eu,Dy phase) exhibited the strongest photoluminescence intensity among the three SAED samples investigated, as indicated by the PL spectra shown in Fig. 6. The observed deterioration in PL intensity of BSAED-LT and

SAED-HT can be attributed to their poor crystallinity (inherited from sol-gel synthesis) and the presence of impurity phases, such as strontium aluminates (i.e., $Sr_3Al_2O_6$ and $SrAl_{12}O_{19}$ for SAED-HT) and/or strontium borates (for BSAED-LT), as indicated by SEM morphological studies and XRD data shown in Figs. 3 and 4, respectively.

F. Comparison of afterglow intensity

To further investigate the effect of boron addition on the initial phosphorescent intensity (I_o) of emission peaks with λ in the range of 483–501 nm for SAED-LT, SAED-HT, BSAED-LT, BSAED-HT, and LumiNova® BG-300M phases, initial intensity I_o was measured and compared (Fig. 7). We have found that BSAED-LT exhibits the strongest phosphorescence intensity among the five samples investigated, even stronger than that of LumiNova® BG-300M. On the other hand, the boron-free SAED phases show the weakest I_o among all. The synthetic temperature adopted for the synthesis and microstructure of the two BSAED samples investigated in this work were found to be critical in determining the initial I_o values. For instance, the BSAED-LT phase (without showing seriously melting morphology) prepared at 800 °C and heated at 1300 °C under reducing atmosphere (5% H_2/95% N_2) for 1 h, exhibits stronger I_o than that for BSAED-HT (showing completely melting morphology) synthesized at 1200 °C for 24 h and further sintered under similar reducing conditions for 1 h.

The comparison of phosphorescent intensity with emission peaking at wavelengths in the range of 483–501 nm for SAED and BSAED phases indicates that boron addition tends to enhance the phosphorescent intensity as well as the I_o value of the SAED phase. These observations are assumed to be correlated with higher Eu^{2+} concentration in BSAED phase due to the effect of boron addition, compared to that in SAED phases. However, a relevant rationalization regarding the enhanced phosphorescent intensity for BSAED phases compared to that for SAED phases requires further investigations.

G. Afterglow decay profile and decay rate

On the other hand, the time-dependent afterglow decay profile during the first five minutes (between 0 and 300 s) for boron-free SAED-HT, boron-added BSAED-LT, and LumiNova® BG-300M (identified as $Sr_4Al_{14}O_{25}$:Eu,Dy phase) were measured and are represented in Figs. 8(a) to 8(c) for comparison, respectively. Regarding the phosphorescent afterglow mechanism of $SrAl_2O_4:Eu^{2+},Dy^{3+}$, through a nonisovalent substitution (Dy^{3+} for Sr^{2+}), the codoping of Dy^{3+} may promote the formation of hole traps in $SrAl_2O_4:Eu^{2+}$ in which Eu^{2+} exhibits a broad $4f^65d–4f^7$ transition as a luminescent center. Ohta *et al.*[20] reported that a hole trap may be ascribed to the Sr^{2+} defects of host lattice that are believed to be stabilized by a charge compensation upon Dy^{3+} doping. On the contrary, an electron trap probably originates from oxygen defects formed when the samples of SAED or BSAED were sintered in a reducing atmosphere during the synthesis. In this investigation we found that the trapping of codoped Dy^{3+} apparently becomes efficacy in all samples heated at 1300 °C under a H_2/N_2 (5%:95%) atmosphere.

As shown in Figs. 8(a) and 8(b), the emission maximum was found to peak mainly at λ_{em} of 486.5 nm for boron-free SAED-HT and a doublet peaking at λ_{em} of 403 and 485 nm for boron-added BSAED-LT. On the other hand, the afterglow peaks of LumiNova® BG-300M whose time-dependent afterglow decay profile shown in Fig. 8(c) was found to be a doublet centering at λ_{em} of 400 and 482 nm. The wavelengths of afterglow peaks for BG-300M were found to be extremely close to those observed in BSAED-LT. Furthermore, the relative intensity ratio of afterglow peaks observed at 400 ± 1 nm

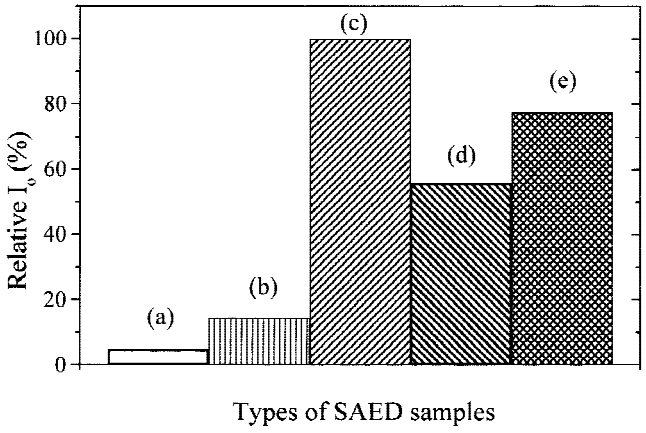

FIG. 7. Comparison of initial phosphorescence intensity (*I*INFo) at λ_{em} = 485 ± 2 nm for (a) SAED-LT, (b) SAED-HT (c) BSAED-LT, (d) BSAED-HT, and (e) BG-300M.

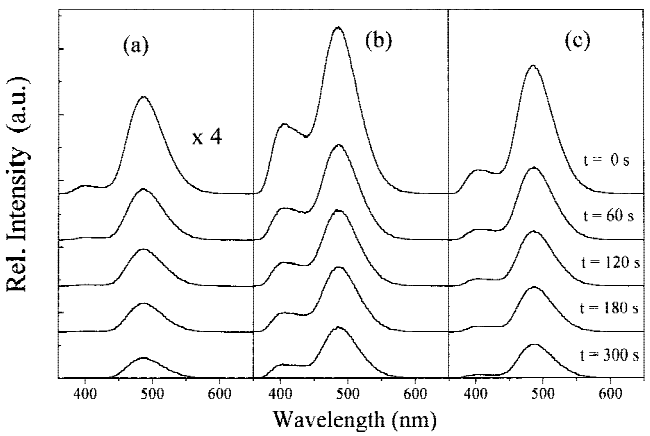

FIG. 8. Comparison of time-dependent afterglow decay profiles for (a) SAED-HT, (b) BSAED-LT, and (c) BG-300M

and 482 ± 1 nm for BSAED-LT and BG-300M, respectively, was found to change in a nonsystematic fashion with time. This finding on the afterglow decay behaviors may suggest that the observed afterglow from twin peaks of BSAED-LT and BG-300M may be rationalized by considering contributions from at least two types of hole or electron traps with different trap energy in the boron-added phases[11] or simply from different aluminates or borates containing Eu^{2+}. The two afterglow peaks observed in BSAED-LT and LumiNova® BG-300M can probably be attributed to the presence of at least two types of traps of similar origin in both samples.

Regarding the time-dependent relative afterglow intensity shown in Fig. 8, we observed that boron-free SAED-HT exhibited the weakest intensity and fastest decay rate, whereas the boron-added BSAED-LT exhibited the strongest intensity, yet slowest decay rate among the three samples of $SrAl_2O_4$:Eu,Dy investigated. The observed enhancement of afterglow intensity due to boron addition was clearly found in BSAED-LT, as compared to that of SAED-LT and LumiNova® BG-300M, indicated by Figs. 8(a) to 8(c).

Furthermore, the nonexponential afterglow decay rate for SAED-LT, SAED-HT, BSAED-LT, BSAED-HT, and LumiNova® BG-300M phases was also investigated and represented in Fig. 9. Essentially, the features of different decay rates in different time periods for all the afterglow decay curves shown in Fig. 9 indicate the presence of various types of traps with different depths in the samples.

Furthermore, the reduced afterglow decay rate derived from the plot of log I/I_0INFo versus time (Fig. 9) was found to be smallest for the boron-added BSAED-LT and BSAED-HT phases, and LumiNova® BG-300M, whereas boron-free SAED-LT and SAED-HT phases showed the fastest decay rates among the five samples. That is, BSAED-LT and BSAED-HT exhibited much longer phosphorescent afterglow than boron-free samples and LumiNova® BG-300M. The observed enhancement of afterglow intensity and lengthening of afterglow rate for boron-added BSAED-LT and BSAED-HT can be attributed to the increasing number of defects due to H_2/N_2 reduction and a higher concentration of Eu^{2+} that was presumably stabilized in a certain type of borate structure in the BSAED. Furthermore, the observed diversity of Eu^{2+} afterglow is probably related to the Eu^{2+} luminescence centers distributed in miscellaneous strontium borates or aluminate phases that may exhibit different strengths of crystal field or different Eu^{2+} coordination environments. Rationalizations for these observations will require thermoluminescence, photoconductivity, and defect investigations and deeper understanding on the decay mechanism.

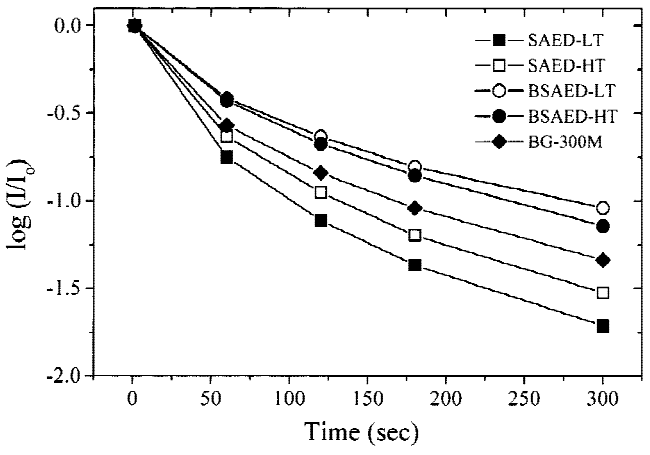

FIG. 9. Comparison of afterglow decay rate for $SrAl_2O_4$:Eu,Dy phases synthesized under different conditions.

IV. CONCLUSIONS

We demonstrated an effective sol-gel route leading to the formation of a bluish-green phosphorescent $SrAl_2O_4$:Eu,Dy phosphor with long afterglow property. We found that boron or borates added into the synthetic reaction of $SrAl_2O_4$:Eu,Dy not only acts as a flux but also enhances the phosphorescent intensity and lengthening of afterglow duration.

Furthermore, the afterglow intensity and decay rate for BSAED phases were found to be enhanced and lengthened upon boron addition. SEM investigations on boron-added BSAED phases suggested that partial or completely melting characters be considered related to the observed enhanced phosphorescence and afterglow intensity and lengthening of decay rate.

ACKNOWLEDGMENTS

The research was supported by the National Science Council of Taiwan, Republic of China, under Contract No. NSC89-2113-M-009-014. We are indebted to Dr. Spring Yeh for her continuous assistance with software used in some of the measurements of long-phosphorescent phosphors. The Industrial and Technology Research Institute (ITRI) is acknowledged for providing part of the facilities used for phosphor synthesis and microstructure characterizations.

REFERENCES

1. G. Blasse and A. Bril, Philips Res. Repts. **23,** 201 (1968).
2. F.C. Palilla, A.K. Albere, and M.R. Tomkus, J. Electrochem. Soc. Solid State Scien.**115**, 642 (1968).
3. Y. Murayama, N. Takeuchi, Y. Aoki, and T. Matsuzawa, U.S. Patent No. 5 424 006 (1995).
4. T. Matsuzawa, Y. Aoki, N. Takeuchi, and Y. Murayama, J. Electrochem. Soc. **143,**2670 (1996).

5. T. Katsumata, T. Nabae, K. Sasajima, S Kumuro, and T. Morikawa, J. Am.Ceram. Soc. **81,** 413 (1998); T. Katsumata, T. Nabae, K. Sasajima, S Kumuro, andT. Morikawa, J. Electrochem. Soc. **144,** L243 (1997).
6. R. Sakai, T. Katsumata, S. Komuro, and T. Morikawa, J. Luminescence **85,** 149 (1999).
7. W. Jia, H. Yuan, L. Lu, H. Liu, and W.M. Yen, J. Luminescence **76&77,** 424 (1998).
8. H. Lange, U.S. Patent No. 3 294 699 (1966).
9. N.A. Sirazhiddinov and P.A. Arifov, Russ. J. Inorg. Chem. **16,** 40 (1971).
10. R.J. Pet, M. van den Nieuwenhof, and J.P.H.M. Duisters, U.S. Patent No. 4 795 588 (1989).
11. I-C. Chen and T-M. Chen, J. Mater Res. (submitted, 2000).
12. R. Nass and H. Schmidt, J. Non-Cryst. Solids **121,** 329 (1990).
13. G. Blasse, J. Solid State Chem. **62,** 207 (1986).
14. Z. Pei, Q. Zeng , and Q. Su, J. Phys. Chem. Solids. **61,** 9 (2000).
15. K. Machida, G.Adachi, and J.Shiokawa, J. Luminescence **21,** 101 (1979).
16. J.Y. Sun, C.S. Shi, and Y.M. Li, Chinese Sci. Bull. **34,** 703 (1989).
17. J. Qiu, K. Miura, N. Sugimoto, and K. Hirao, J. Non-Crystalline Solids. **213&214,** 266 (1997).
18. G. Blasse in *Luminescence of Inorganic Solids* , edited by B.O. Bartolo (PlenumPress, New York, 1978), p. 463.
19. Von A-R. Schulze, Hk. Müller-Buschbauch, Z. Anorg. Allg. Chem. **475,** 205 (1981).
20. M. Ohta, M. Maruyama, T. Hayakawa, and T. Nishijo, J. Ceram. Soc. Japan **108,**284 (2000).